Photoelectrochemistry of Pristine Mono- and Few-layer MoS2

DOI:
10.1021/acs.nanolett.5b05317

Document Version
Final published version

NANO LETTERS

Letter

pubs.acs.org/NanoLett

Photoelectrochemistry of Pristine Mono- and Few-Layer MoS_2

Matěj Velický,*[,†] Mark A. Bissett,[†] Colin R. Woods,[‡] Peter S. Toth,[†] Thanasis Georgiou,[§] Ian A. Kinloch,[∥] Kostya S. Novoselov,[‡] and Robert A. W. Dryfe*[,†]

[†]School of Chemistry and [‡]School of Physics and Astronomy, University of Manchester, Oxford Road, Manchester, M13 9PL, United Kingdom

[§]Manchester Nanomaterials Ltd., 83 Ducie Street, Manchester, M1 2JQ, United Kingdom

[∥]School of Materials, University of Manchester, Oxford Road, Manchester, M13 9PL, United Kingdom

Supporting Information

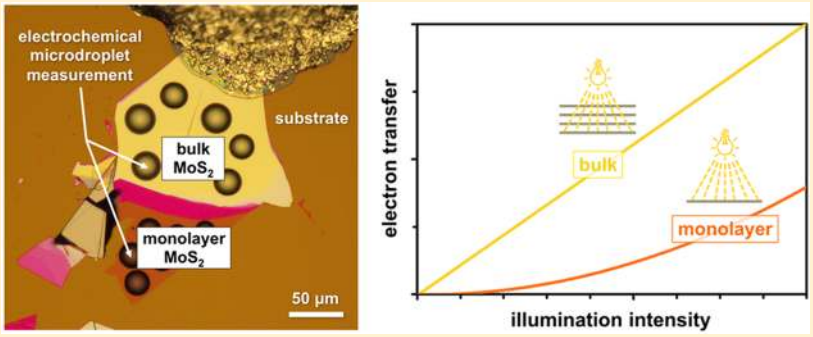

ABSTRACT: Two-dimensional crystals are promising building blocks for the new generation of energy materials due to their low volume, high surface area, and high transparency. Electrochemical behavior of these crystals determines their performance in applications such as energy storage/conversion, sensing, and catalysis. Nevertheless, the electrochemistry of an isolated monolayer of molybdenum disulfide, which is one of the most promising semiconducting crystals, has not been achieved to date. We report here on photoelectrochemical properties of pristine monolayer and few-layer basal plane MoS_2, namely the electron transfer kinetics and electric double-layer capacitance, supported by an extensive physical and chemical characterization. This enables a comparative qualitative correlation among the electrochemical data, MoS_2 structure, and external illumination, although the absolute magnitudes of the electron transfer and capacitance are specific to the redox mediator and electrolyte used in these measurements ($[Ru(NH_3)_6]^{3+/2+}$ and LiCl, respectively). Our work shows a strong dependence of the electrochemical properties on the number of MoS_2 layers and illumination intensity and proves that an effective interlayer charge transport occurs in bulk MoS_2. This highlights the exciting opportunities for tuning of the electrochemical performance of MoS_2 through modification of its structure, external environment, and illumination.

KEYWORDS: *Molybdenum disulfide, two-dimensional, electron transfer, capacitance, illumination*

Molybdenum disulfide has been the flagship material in the research of two-dimensional (2D) materials beyond graphene.[1] The main use of MoS_2 as a solid lubricant[2] has been extended to research in optoelectronics, photovoltaics, and sensors,[3] following the recent boom in 2D materials. Devices fabricated from thin layers of pristine MoS_2 have recently been shown to have excellent charge carrier mobility (>30,000 $cm^2 V^{-1} s^{-1}$),[4] and even exhibit superconducting behavior under sufficiently high doping.[5] MoS_2 is a semiconducting member of a large family of layered transition metal dichalcogenides (TMDCs)[6] with a indirect−direct band gap transition between bulk (∼1.2 eV) and monolayer (∼1.8 eV) form.[7] Mono- and few-layer MoS_2 preparation methods include the "scotch-tape" mechanical exfoliation[8] and liquid-phase exfoliation of natural molybdenite crystals[9] and also synthetic routes such as chemical vapor deposition (CVD),[10] or hydrothermal growth.[11]

A large portion of MoS_2 research focuses on applications in energy storage and conversion including batteries,[12] solar cells,[13] supercapacitors,[14] and fuel cells.[15] Electron transfer (ET) kinetics and electric double-layer capacitance (EDLC) are the two key electrochemical properties, which determine performance of MoS_2 in these applications. While bulk MoS_2 has been studied to some extent,[16−19] there is a clear lack of electrochemical knowledge on mono- or few-layer MoS_2. Recently, electrochemistry of thin layers of liquid-phase exfoliated MoS_2 has been reported and shown to be significantly affected by the method of preparation.[20,21] Liquid-exfoliated materials, however, behave differently than pristine MoS_2, and, exhibit inferior electrochemical perform-

Received: December 31, 2015
Revised: January 28, 2016
Published: February 3, 2016

DOI: 10.1021/acs.nanolett.5b05317
Nano Lett. 2016, 16, 2023−2032

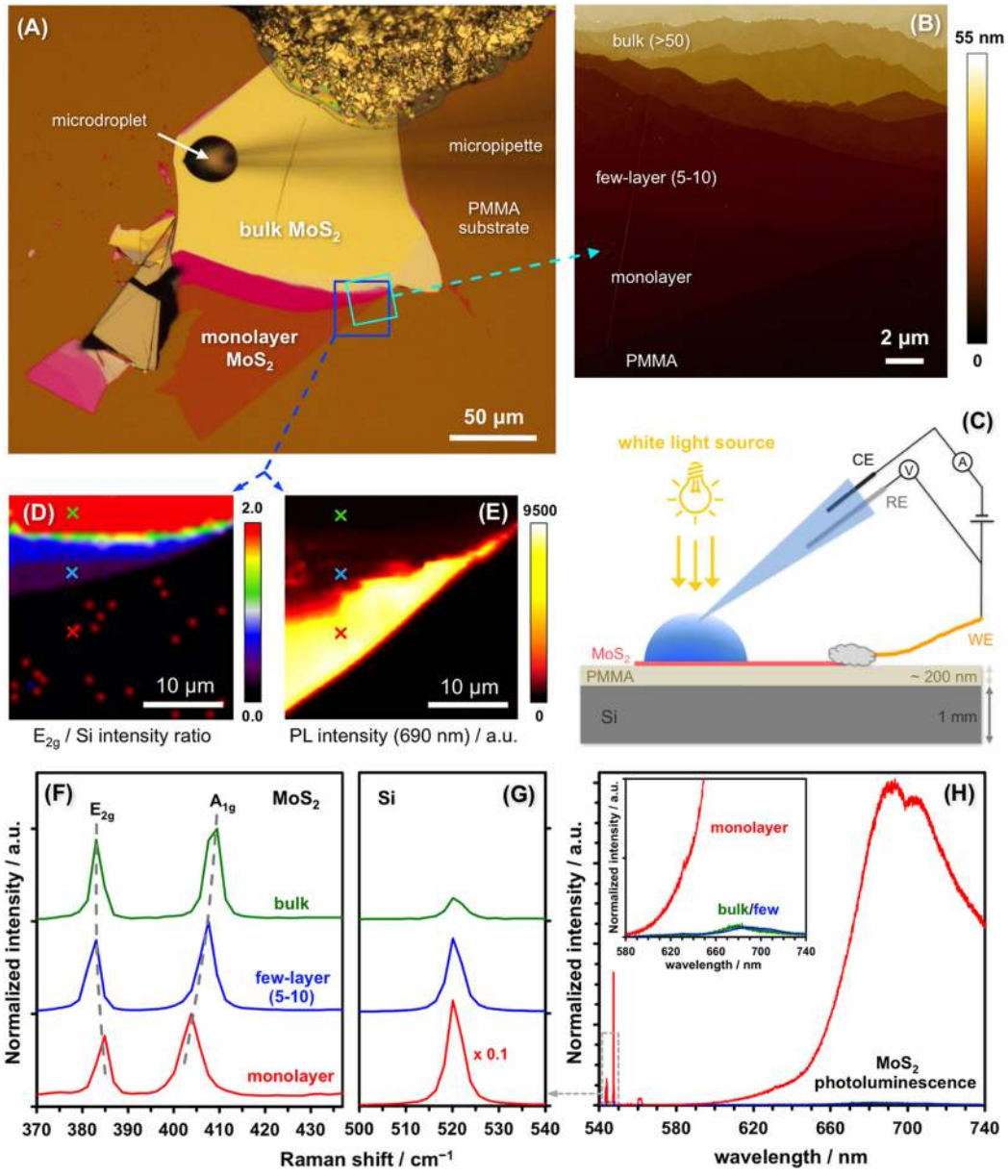

Figure 1. Optical microscopy, AFM, photoelectrochemical setup, Raman spectroscopy, and PL measurement of MoS_2 layers. (A) Optical micrograph of an MoS_2 flake on PMMA-coated Si substrate. (B) AFM micrograph of a selected monolayer/few-layer/bulk flake region. (C) Schematic of the photoelectrochemical setup. (D) Raman map of the E_{2g}/Si intensity ratio. (E) PL intensity map at 690 nm wavelength. (F) and (G) Raman spectra showing the two main MoS_2 bands and the Si band, respectively, and their evolution with the number of MoS_2 layers. (H) PL spectra of the monolayer/few-layer/bulk MoS_2. The areas used for the AFM measurement (B) and the Raman (D) and PL (E) maps are indicated in (A) by light blue and dark blue squares, respectively. The Raman and PL spectra of (F−H) were recorded at spots indicated by colored crosses in (D,E), respectively.

ance due to the small lateral size of the flakes, solvent residues, and impurity adsorbates. CVD-grown MoS_2 has recently been shown to have thickness-dependent activity toward hydrogen evolution reaction.[22] Importantly, electrochemical response of a pristine, isolated monolayer MoS_2 crystal has not been reported to date. This lack of fundamental work is most likely linked to difficulties in preparation, which has been the main reason for limited research on mechanically exfoliated graphene.[23−27]

In this work, we isolate and characterize high-quality, pristine MoS_2 monolayers and multilayers, and measure the ET kinetics and EDLC of their basal planes in aqueous electrolyte solutions. The magnitude of these key electrochemical properties increases with the surface density of electronic states (DOS), reflects surface oxidation or contamination, and is also an indirect measurement of the MoS_2 conductivity. ET kinetics especially can vary over a several orders of magnitude due to these factors with its absolute value depending on the self-exchange rate of the selected redox mediator. In this study, we use a $[Ru(NH_3)_6]^{3+/2+}$ outer-sphere redox mediator, which is believed to be a nonadsorbing molecule insensitive to surface groups, meaning that the relative changes in its ET kinetics reflect the differences in the DOS of MoS_2.[28] Atomically thin MoS_2 layers are prepared using mechanical exfoliation of natural molybdenite crystals on a polymer-coated silicon substrate, yielding flakes of relatively large lateral dimensions, up to several hundred micrometers. A range of techniques

DOI: 10.1021/acs.nanolett.5b05317
Nano Lett. 2016, 16, 2023−2032

including optical microscopy, Raman spectroscopy, photoluminescence (PL) measurement, atomic force microscopy (AFM), and X-ray photoelectron spectroscopy (XPS) were employed to determine the thickness of the MoS_2 flakes, surface quality, and chemical composition. Localized photoelectrochemical measurement on individual single-crystals was carried out under white light illumination of a controlled intensity. Both electron transfer and capacitance are shown to depend on the number of MoS_2 layers, which is a direct consequence of the thickness-dependent light absorption and subsequent photogeneration of free charge carriers.

Results and Discussion. *Physical and Chemical Characterization of MoS_2.* Figure 1 summarizes the main characterization techniques. High optical contrast on a Si wafer coated with a thin layer of poly(methyl methacrylate) (PMMA) allows MoS_2 flakes of all thicknesses to be located and visualized using optical microscopy (Figure 1A). The thickness of few-layer (5−10) and bulk MoS_2 flakes can reliably be determined using AFM (Figure 1B) but the thinnest flakes (1−3) suffer from adventitious adsorbates and flake-substrate equilibrium separation,[29,30] which increase their AFM-derived thickness by 0.5−1.0 nm (Supporting Figure S1). Foreign adatoms on thin MoS_2 crystals causing such discrepancies were first observed by Frindt,[31] and more recently, hydrocarbon adsorbates, directly affecting the electrochemical performance of MoS_2 have been confirmed.[19] An aqueous microdroplet of electrolyte solution was placed on the MoS_2 basal plane surface using an electrically controlled micropipette, allowing a localized measurement of electron transfer and capacitance at the MoS_2/liquid interface in a standard three-electrode configuration (Figure 1A,C). White light illumination was used to generate free charge carriers in the semiconducting MoS_2 (irradiance calibration curves are shown in Supporting Figure S2). Optical microscopy and AFM were complemented with Raman spectroscopy and PL measurement, which, as shown in Figure 1D−H, reliably distinguish between mono-, bi-, trilayer and thicker flakes. The two most intense Raman phonon modes, corresponding to the in-plane (E_{2g}) and out-of-plane (A_{1g}) lattice vibrations, exhibit hardening and softening, respectively, when transitioning from bulk to monolayer MoS_2 (Figure 1F).[32] The A_{1g}−E_{2g} Raman shift difference was used for an accurate determination of the number of layers using an appropriate calibration (Supporting Figure S3). The 520 cm^{-1} Raman mode of the underlying Si, which is ∼10 times more intense for monolayer than few-layers (5−20) and further diminishes for bulk MoS_2 (>50 layers), was also used to assess the flake thickness (Figure 1G). Furthermore, the PL of a monolayer is about 100× more intense than that of the bulk crystal, as demonstrated in Figure 1H. Figure 1D,E shows the Raman E_{2g}/Si intensity ratio and PL maps of the selected regions in Figure 1A. The dependencies of the Si Raman and MoS_2 PL intensity on the flake thickness are shown in Supporting Figure S4. Characterization of the flake surface using XPS (high-resolution spectra and imaging) confirmed that MoS_2 is of semiconducting 2H phase with Mo and S being the major element components (Supporting Figures S5 and S6). Only minor differences between the XPS spectra of monolayer and bulk MoS_2 flakes were found. This comprehensive surface and photoelectrochemical characterization allows unambiguous assessment of the electrochemical performance of MoS_2 and unraveling of its dependence on MoS_2 thickness and external illumination.

Dependence of Electron Transfer on the Number of MoS_2 Layers and Illumination. The ET kinetics of $[Ru(NH_3)_6]^{3+/2+}$ reduction/oxidation in aqueous solution at an MoS_2 surface, expressed as the standard heterogeneous ET rate constant (k^0) was determined from the peak-to-peak separation between the resultant reduction and oxidation waves (Figure 2A). [Ru-

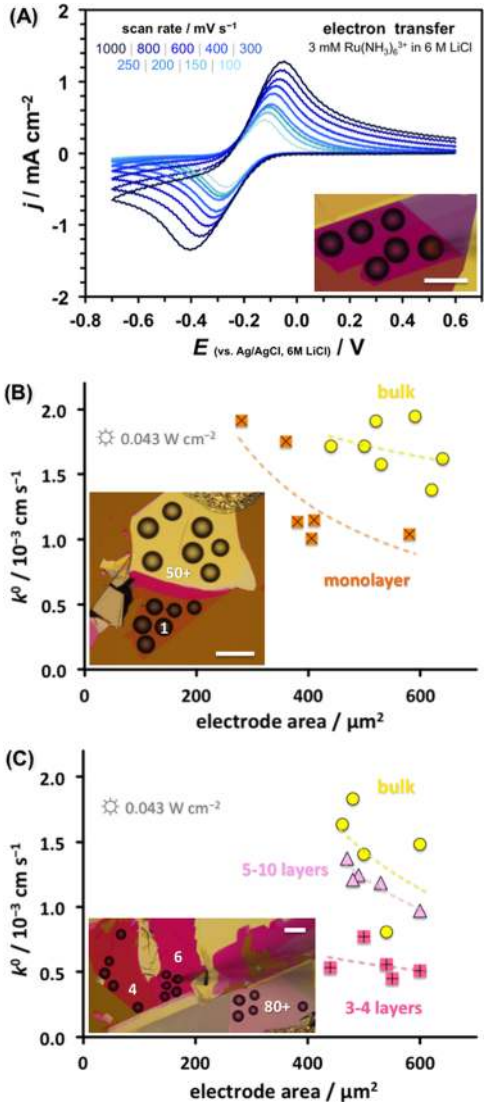

Figure 2. Electron transfer kinetics measurement. (A) Cyclic voltammograms of $[Ru(NH_3)_6]^{3+/2+}$ reduction/oxidation for the ET kinetics determination. (B,C) Heterogeneous ET rate constants (k^0) for samples B and C, respectively. The ET kinetics (and also EDLC) are shown to be inversely proportional to the working electrode area due to light absorption effects (Supporting Figures S8 and S9). Plotting k^0 against the electrode area thus aids a direct comparison between layers of different thicknesses. The insets show optical micrographs of the individual droplet measurements, all scale bars denote 50 μm. The ET kinetics measured on some few-layer samples also depend on the distance from an electrical contact to a flake due to low conductivity of thin MoS_2 (Supporting Figure S10).

$(NH_3)_6]^{3+/2+}$ is an outer-sphere redox mediator, which is thought to be insensitive to any surface functional groups and only to reflect the changes in the DOS of the electrode material. The k^0 was calculated from eq 1 for peak-to-peak separation, ΔE_p, > 220 mV, or eq 2 for ΔE_p < 220 mV. An explicit expression for k^0 is[33]

DOI: 10.1021/acs.nanolett.5b05317
Nano Lett. 2016, 16, 2023−2032

$$k^0 = 2.18\left(\frac{\alpha z F D \nu}{RT}\right)^{1/2} e^{(\alpha^2 F/RT) z \Delta E_p} \quad (1)$$

where α is the transfer coefficient (here assumed to be 0.5 due to the reaction symmetry), $z = 1$ is the number of electrons exchanged in the reaction, F is the Faraday constant, D is the diffusion coefficient of the redox mediator, ν is the scan rate, R is the universal gas constant, and T is the thermodynamic temperature. The Nicholson method, based on a normalized kinetic parameter, ψ, and its scan rate dependence, was also used[34]

$$\psi = k^0 \sqrt{\frac{RT}{\pi n F D}} \nu^{-0.5} \quad (2)$$

In this case, $\psi - \Delta E_p$ working function was used to determine ψ and then directly calculate k^0[35]

$$\psi = \frac{(-0.6288 + 0.0021 z \Delta E_p)}{(1 - 0.017 z \Delta E_p)} \quad (3)$$

Voltammetry at scan rates between 0.1 and 1 V s^{-1} was performed for each droplet (Figure 2A) and mean k^0 value determined using the analytical methods above. It is important to note that the absolute value of ET kinetics measured here is specific to the selected $[Ru(NH_3)_6]^{3+/2+}$ redox mediator used in these measurements.

Natural 2D crystals often contain atomic vacancies, trace impurities, and adsorbates, which can all act as effective dopants.[36,37] The related sample-to-sample variation of MoS_2 electrical properties is a common problem, which has been linked to various causes including defects, adsorbed water, and MoS_2/metal contact resistance,[38−41] and confirmed here by the heterogeneity of the Raman and PL spectra across a monolayer MoS_2 (Supporting Figure S7). Electrochemical response of the semiconducting MoS_2, especially, is sensitive to illumination, as shown previously for bulk MoS_2.[16,17,19] We have therefore specifically chosen to compare the responses of the directly adjacent parts (i.e., monolayer, few-layer, and bulk flakes) of a single-crystal MoS_2 domain.

The single-crystal nature of these connected flakes, along with the constant illumination intensity, allow correlation between the electrochemical performance and number of MoS_2 layers to be unraveled in a reliable fashion. Such an approach guarantees sample homogeneity and a reliable analysis. Figure 2B−C show the ET kinetics (k^0) determined for monolayer, few-layer and bulk flakes of two different MoS_2 samples (B and C). All 91 individual measurements performed across 8 different MoS_2 samples (A − H) are shown in Supporting Figure S11. The ET kinetics vary significantly between each sample with maximum and minimum k^0 values being 1.95×10^{-3} cm s^{-1} for bulk MoS_2 (sample B) and $\sim 10^{-8}$ cm s^{-1} for monolayer MoS_2 (sample G).

Importantly, the ET kinetics are found to increase systematically with increasing flake thickness, despite the sample-to-sample variation described above. This is evident from measurements under differing illumination intensity, which reveal dependence of the ET kinetics on the irradiance for both monolayer and bulk MoS_2, as shown in Figure 3A. Two main conclusions can be drawn from this graph: (1) bulk MoS_2 exhibits faster ET kinetics than the monolayer MoS_2; (2) while the ET kinetics of bulk MoS_2 is linearly dependent on the irradiance, monolayer MoS_2 shows stronger, nonlinear dependence on irradiance. The differences between the kinetics on

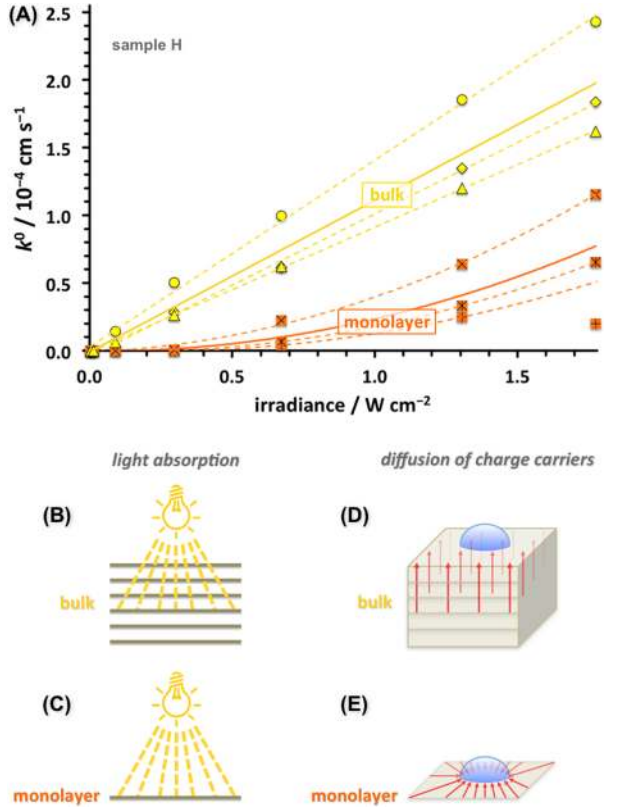

Figure 3. Electron transfer kinetics on monolayer and bulk MoS_2. (A) Dependence of the monolayer and bulk MoS_2 ET kinetics (k^0) on irradiance, determined from individual droplet measurements (sample H). Orange and yellow correspond to monolayer and bulk MoS_2, respectively, the dashed lines/curves are the best fits for the individual droplet measurements, and the solid lines represent the averaged response. (B,C) Schematic diagrams demonstrating the efficiency of incident light absorption in bulk and monolayer MoS_2, respectively. (D,E) Schematic diagrams showing the different charge carrier diffusion profiles in bulk and monolayer MoS_2, respectively.

bulk and monolayer flakes can be explained by the total light absorption, which strongly depends on the number of MoS_2 layers. While a single S−Mo−S layer only absorbs a small fraction of the incident light and therefore generates only a limited amount of free charge carriers contributing to the ET kinetics, many more S−Mo−S layers can convert the incident photons to a significant amount of charge carriers in bulk MoS_2, as schematically shown in Figure 3B,C. On the other hand, the nonlinear kinetics-irradiance dependence in monolayer MoS_2 is an unexpected observation. We explain this phenomenon by the fundamental difference in the diffusion of charge carriers within the bulk and monolayer MoS_2, as shown in Figure 3D,E. The majority of the incident light (>99%) is absorbed in the top 50 layers (~30 nm), as determined from eq 6 considering the optical absorption of monolayer MoS_2 to be ~10% (the exact value depending on the reflectivity of an underlying substrate).[42−44] As the light penetrates well inside the bulk MoS_2 and generates charge carriers, which are electrochemically consumed at the top MoS_2 layer, a linear diffusion profile is established between the deepest light-absorbing layer and MoS_2 surface (Figure 3D). This results in a linear dependence of k^0 on the total radiant flux; the growing irradiance linearly increases the light penetration depth and concentration of the charge carriers within the top MoS_2 layer. This also confirms

DOI: 10.1021/acs.nanolett.5b05317
Nano Lett. 2016, 16, 2023−2032

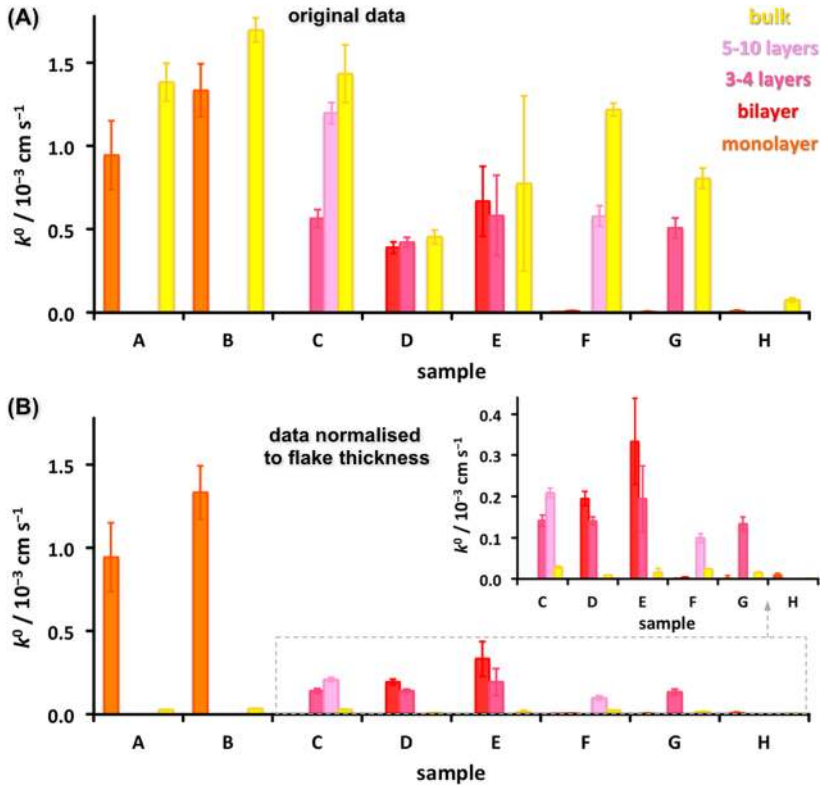

Figure 4. Correlation between the electron transfer kinetics and MoS_2 thickness. (A) ET rate constant (k^0) determined for MoS_2 samples with varied flake thickness. (B) Same correlation but with the k^0 normalized to the number of MoS_2 layers. To normalize all of the bulk data, n = 50 layers was used in accordance with the discussed >99% light absorption in bulk MoS_2.

that an effective interlayer transport of charge carriers occurs between the individual sheets of MoS_2, which is in contrast to recent observations.[45] On the other hand, in monolayer MoS_2 the diffusion of the charge carriers is only limited to a single light-absorbing sheet. This results in a radial charge carrier diffusion profile (Figure 3E) and consequent nonlinear (parabolic) dependence of k^0 on irradiance. It was beyond the scope of this study to develop a fully quantitative model describing the dependence of k^0 (or other electrochemical function) on the number of layers. However, it is our hope that this will be the focus of future studies on the photoelectrochemistry of layered semiconducting materials.

Figure 4 summarizes all k^0 values measured for the samples A–H as a function of the MoS_2 thickness. For the sake of simplicity, the flake thickness was categorized into the following five different groups: monolayer, bilayer, 3–4 layers, 5–10 layers, and bulk (50+ layers). Although we were not able to establish a quantitative relationship between the interlayer charge carrier transport ($CT_{interlayer}$) and electron transfer between the top-layer MoS_2 and $[Ru(NH_3)_6]^{3+/2+}$ ($CT_{surface}$), it seems plausible to infer that $CT_{surface}$ is faster for MoS_2 flakes of high intrinsic conductivity than for the low conductivity ones (samples A and H in Figure 4 are examples of the former and latter case, respectively). The fact that the absolute ET kinetics of bulk MoS_2 is always faster than that of mono- and few-layer MoS_2 suggests that $CT_{surface}$ (and not $CT_{interlayer}$) is the limiting factor for the photoelectrochemical reaction. Figure 4A,B shows a comparison between the original kinetics data and the kinetics normalized to the number of MoS_2 layers, respectively. This provides a useful assessment of the performance of MoS_2 in relation to the quantity of the electrode material, that is, volume, mass, or active area.

Although the ET kinetics is an intensive physicochemical property, the normalization per thickness highlights that electrochemistry is limited to the top MoS_2 layer, while the bulk only contributes to the interlayer transport of photogenerated charge carriers and does not actively participate in the electrochemical process. This is a solid justification for exfoliation of bulk MoS_2 to thin flakes for energy storage/conversion applications and it points toward a few-layer (5–10) MoS_2 as a good compromise between a high surface area and a sufficiently fast ET.

It is also useful to analyze the absolute kinetics of the $[Ru(NH_3)_6]^{3+/2+}$ redox reaction at different semimetallic and metallic surfaces. The $[Ru(NH_3)_6]^{3+/2+}$ ET kinetics, determined via the same experimental method used here, increase as follows ($k^0/10^{-3}$ cm s^{-1}):[24] natural graphite, 0.053; highly ordered pyrolytic graphite, 0.35, best performing MoS_2 (bulk, under illumination), 1.7 (this work); Pt, 3.4; and Au, 3.7. Note that these are values for surfaces aged in air for more than 24 h, and that in the case of freshly cleaved graphite and MoS_2 the $[Ru(NH_3)_6]^{3+/2}$ ET kinetics are comparable to those of unpolished Pt and Au.[19,24] The above analysis shows that the magnitude of light-activated ET on natural MoS_2 can be comparable with metallic electrodes.

Relationships among Capacitance, Electron Transfer, MoS_2 Thickness, and PL. The capacitance was determined from the voltammetric background current measurement in a 6 M LiCl supporting electrolyte aqueous solution within a potential window of 0.5 V where no faradaic processes occurred (Figure 5A). The electric double-layer capacitance was calculated from the following equation, adapted from ref 46

DOI: 10.1021/acs.nanolett.5b05317
Nano Lett. 2016, 16, 2023–2032

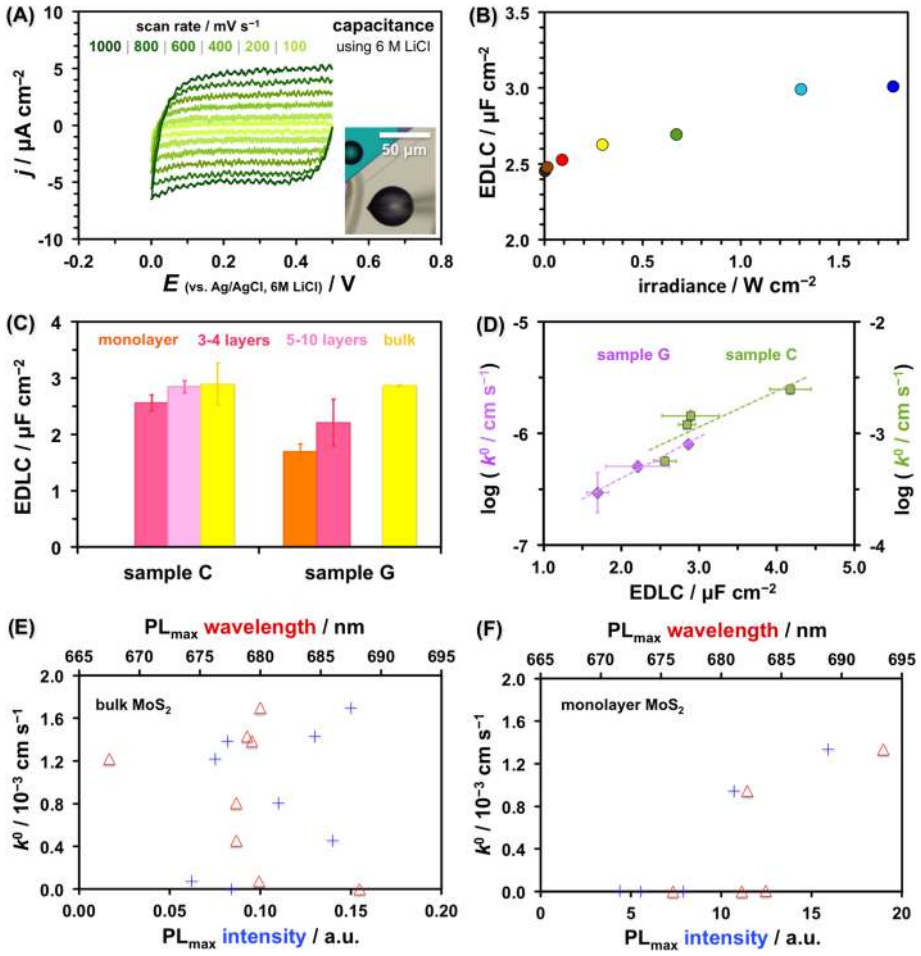

Figure 5. Relationships among capacitance, electron transfer, MoS_2 thickness, and PL. (A) Cyclic voltammograms using 6 M LiCl supporting electrolyte for EDLC determination. (B) Dependence of EDLC on irradiance. (C) Dependence of EDLC on flake thickness determined for two different MoS_2 samples. (D) ET kinetics correlation with EDLC for the same samples. (D,E) ET kinetics versus maximum PL wavelength and maximum PL intensity for bulk and monolayer MoS_2, respectively.

$$\mathrm{EDLC} = \frac{1}{2\nu(E_{\max} - E_{\min})} \oint_E I(E)\mathrm{d}E \tag{4}$$

where E is the applied potential and $E_{\max}$ ($E_{\min}$) are the maximum (minimum) potentials applied during the voltammetric scan. The mean EDLC was determined from several measurements at different scan rates, typically within the range of 0.1−3 V s^{-1}. The EDLC was shown to depend only slightly on the scan rate (Supporting Figure S12).

The EDLC varied between 1.5−5.8 μF cm^{-2} and increased with increasing illumination intensity by ∼20% (from dark to 1.8 W cm^{-2} irradiance, measured at 532 nm), as shown in Figure 5B for bulk MoS_2. Also, sensitivity of the capacitance to illumination is potential-dependent with the largest changes being most pronounced at high potentials, that is, low electron energies (Supporting Figure S13). This is consistent with the n-type doping of natural MoS_2; it behaves as a dark cathode/photoanode and the photoconductive behavior is therefore most prominent at high potentials.[16,17,19] The EDLC also depends on the number of MoS_2 layers, as shown in Figure 5C, which is especially noticeable for the low conductivity sample G. Furthermore, a linear correlation exists between the decimal logarithm of k^0 and EDLC with both values determined on the same surface (Figure 5D). This holds for two samples of differing intrinsic conductivity determined qualitatively from the ET measurement (C, high conductivity, bulk $k^0 \sim 1.43 \times 10^{-3}$ cm s^{-1} at 0.04 W cm^{-2}; and G, low conductivity, bulk $k^0 \sim 0.81 \times 10^{-3}$ cm s^{-1} at 0.67 W cm^{-2}). Interestingly, although a relationship between the ET kinetics and EDLC was previously reported for glassy carbon and highly ordered pyrolytic graphite,[47,48] there is a clear lack of description of an explicit quantitative correlation between these two properties and its fundamental explanation for semimetallic and semiconducting electrodes.[49]

The ET kinetics was also plotted against the maximum intensity and corresponding wavelength of MoS_2 photoluminescence. While the kinetics on bulk MoS_2 (Figure 5E) do not correlate well with the PL wavelength (red triangles), there is a weak underlying trend with the PL intensity (blue crosses). The kinetics of a monolayer MoS_2 (Figure 5F) show a general increasing trend with increasing PL wavelength and intensity, despite the scattered data.

Photocurrent as a Function of MoS_2 Thickness. Further assessment of MoS_2 performance as an electrode can be gleaned from voltammetric measurements in pure electrolyte (6 M LiCl), which are shown in Figure 6. The illumination clearly affects the voltammetry of both MoS_2 samples despite their differing conductivity (C, high and G, low), and significant differences are observed between the monolayer, few-layer, and bulk MoS_2. Let us first discuss the higher conductivity sample

DOI: 10.1021/acs.nanolett.5b05317
Nano Lett. 2016, 16, 2023−2032

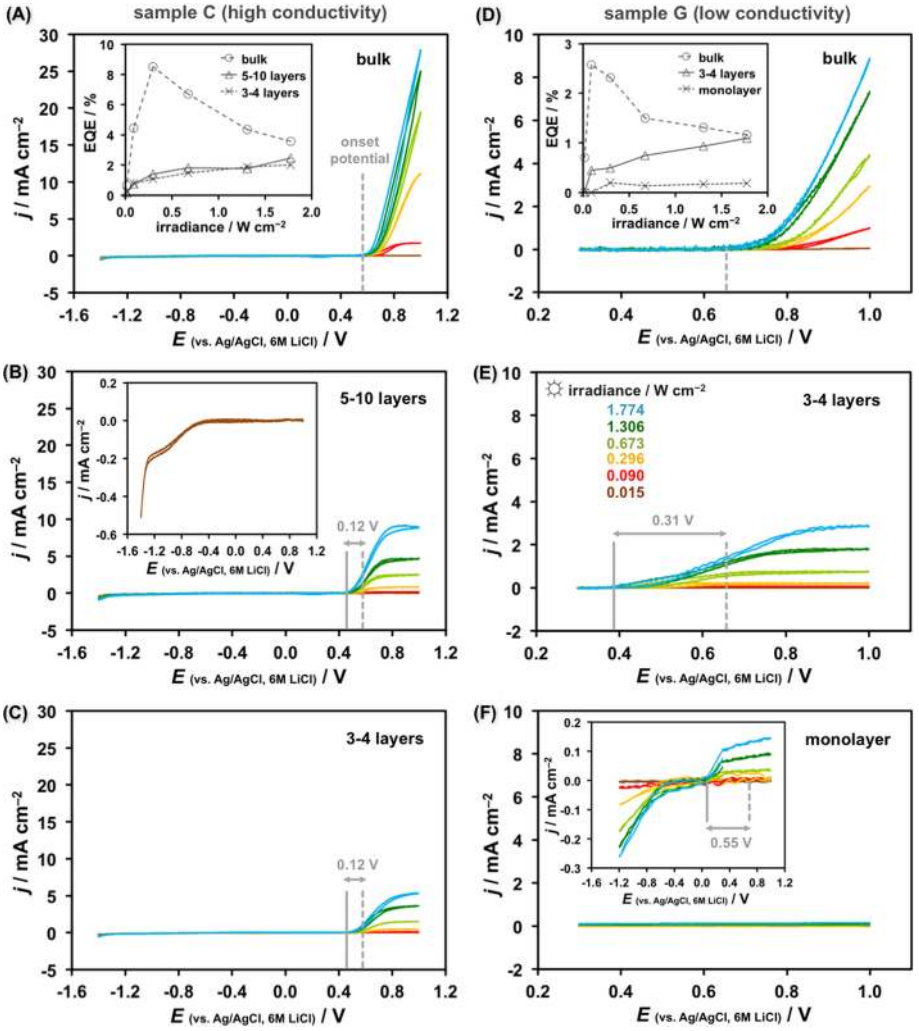

Figure 6. Photoanodic behavior of MoS_2 and its dependence on the number of layers. (A−C) Series of cyclic voltammograms recorded for bulk, 5−10 layers, and 3−4 layers of a high conductivity MoS_2 sample, respectively. (D−F) Positive potential branches of voltammograms recorded on bulk, 3−4 layers, and a monolayer of a low conductivity MoS_2 sample, respectively. The insets in (A,D) show the dependence of the EQE, calculated from eq 5, on the irradiance. The different colors of the voltammetric curves correspond to the different irradiance values shown in (E). Zooms of the lowest-irradiance voltammogram and the low-current monolayer response are shown in the insets of (B,F), respectively.

(Figure 6A−C). A large photocurrent, most likely originating from water oxidation, chloride oxidation and/or sulfate formation,[16,50,51] is observed above 0.6 V for the bulk MoS_2 as shown in Figure 6A. For the irradiance up to ca. 0.3 W cm^{-2}, the photocurrent reaches a plateau, whose height increases with illumination. Above this irradiance, the current increases monotonously with potential. For MoS_2 about 5−10 layers thick, the photocurrent reaches a plateau even for the highest irradiance (1.8 W cm^{-2}) and has ca. 3 × lower magnitude than the bulk (Figure 6B). Further decrease in the photocurrent is observed for MoS_2 3−4 layers thick (Figure 6C). The photocurrent in the lower conductivity sample G, which is on average 2−3 × lower than that of sample C, exhibits slightly different behavior. The bulk MoS_2 photocurrent does not reach a plateau for any of the illumination intensities used. Instead, the photocurrent increases exponentially with the potential, increasing in magnitude with the irradiance (Figure 6D). The photocurrent of 3−4 layer thick MoS_2 reaches a plateau (Figure 6E) and only small photocurrent response is observed for the monolayer MoS_2 due to its poor conductivity (Figure 6F). Importantly, for both samples there is a consistent shift in the photocurrent onset potential between the bulk and thin MoS_2 flakes. In the case of sample C, the onset potential is decreased by ∼0.12 V for thin flakes (3−4 and 5−10 layers) in comparison to bulk MoS_2.

This is much more pronounced for sample G with ∼0.31 V onset potential downshift for 3−4 layers in comparison to bulk MoS_2, and an overall downshift of ∼0.55 V between monolayer and bulk MoS_2. The shift in the onset potential can be interpreted as a direct representation of the difference between the work functions of monolayer and bulk MoS_2 (5.1 and 4.5 eV, respectively).[52] As illustrated with a simplified band diagram in Figure 7, the work functions of monolayer and bulk MoS_2 define their Fermi levels (E_F).[28] The photoanodic oxidation reaction discussed here is represented by a DOS distribution function $D_R(E)$ at the energy level corresponding to the reduced form of a species R at MoS_2/liquid interface. In order to oxidize R, the energy level of the electron receiving states in MoS_2 must be equal or lower than the energy level of the occupied states of R.[28] Figure 7 shows that while the Fermi levels of both monolayer and bulk MoS_2 have to be lowered for the oxidation to proceed, E_F^{mono} requires a smaller shift in

DOI: 10.1021/acs.nanolett.5b05317
Nano Lett. 2016, 16, 2023−2032

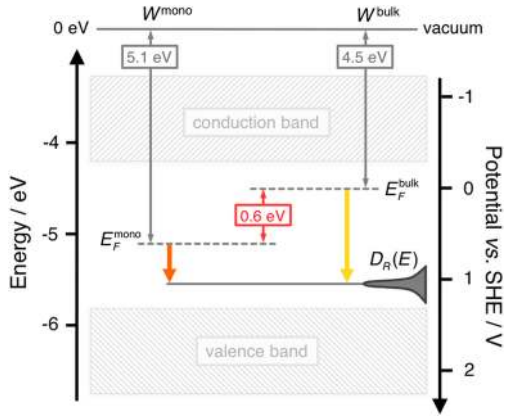

Figure 7. A simplified band diagram illustrating the effect of differing work functions of monolayer and bulk MoS_2 on the oxidation onset potential. The energy levels are approximate and the potential scale is referenced versus the standard hydrogen electrode (SHE).

energy (potential) than E_F^{bulk}. Therefore, an oxidation reaction at MoS_2 surface will proceed more easily on a monolayer than bulk. The onset potential difference of ~0.55 V between monolayer and bulk MoS_2 closely matches the 0.6 eV difference between their work functions. (We should add that the while the exact Fermi level position will be affected by the junction potential at the solid/liquid, the relative difference between E_F^{mono} and E_F^{bulk} arising from the differing work functions should be maintained.) The difference in work functions explains the potential shift well, although we cannot rule out other causes, such as doping effects from the PMMA substrate, which have been shown to affect mobility of MoS_2 over a surprisingly long vertical distances.[41]

Importantly, no significant photocorrosion of mono- and few-layer MoS_2 under high illumination, current, or repeated voltammetric cycling was observed and therefore majority of the photoanodic current in Figure 6 originates from water or chloride oxidation rather than oxidation of the MoS_2 surface. The photocorrosion resistance can be attributed to a stable anodic oxidation mechanism, which is supported by formation of holes in the d-orbitals of Mo, as previously noted for bulk MoS_2.[50] We have also calculated the external quantum efficiencies (EQE) of the incident photon-to-photocurrent conversion, which are shown in the inset of Figure 6A,D as a function of irradiance. The EQE was calculated as

$$\mathrm{EQE}(\%) = 100 \times \frac{N_e}{(1 - T_r)N_{h\nu}} = 100 \times \frac{I_p}{e}\frac{\varepsilon}{(1 - T_r)E_e} \quad (5)$$

where N_e is the number of electrons generated per second, $N_{h\nu}$ is the number of incident photons per second, I_p is the generated photocurrent, e = 1.60217657 × 10^{-19} C is the elementary charge, E_e is the irradiance, and ε is the energy of a single photon quantum, calculated as $\varepsilon = hc/\lambda$, where h = 6.626 × 10^{-34} J s is the Planck constant, c = 2.998 × 10^8 m s^{-1} is the speed of light in air, and λ = 532 nm is an arbitrary photon wavelength. T_r is the transmittance, calculated as

$$T_r = (1 - x)^n \quad (6)$$

where x is the fraction of light absorbed by one layer ($x \approx 0.1$) and n is the number of MoS_2 layers.

The maximum EQE reaches 8.5% for bulk MoS_2 (sample C), which significantly exceeds previously reported values.[16,50,53] Interestingly, while the EQE of thin MoS_2 (<10 layers) decreases monotonously with decreasing irradiance, the EQE of bulk MoS_2 show a maximum between 0.1−0.3 W cm^{-2}, which is close to the solar constant value (see Supporting Figure 2).

This study highlights the critical influence of the number of layers and illumination on electrochemical properties of MoS_2, which in turn affect performance of this material in energy storage/conversion, sensing, and electrocatalysis. We have successfully measured the electron transfer kinetics and capacitance of pristine mono- and few-layer basal plane MoS_2 and found that they both increase with the growing number of MoS_2 layers and increasing irradiance. Our interpretation of these results is based on a multilayer absorption of photons in bulk MoS_2 and subsequent interlayer transport of photogenerated charge carriers, which contributes to the enlarged photoelectrochemical response of bulk MoS_2 in comparison to monolayer MoS_2. The detailed analysis reveals that while the ET kinetics depends linearly on irradiance for bulk MoS_2, a nonlinear behavior is observed for monolayer MoS_2. This is explained by differing diffusion mechanism of charge carriers within monolayer and bulk MoS_2. It should be noted that although the relative changes in the ET kinetics reflect differences in the electrochemical activity of MoS_2, the ET kinetics absolute value is determined by the self-exchange rate of the $[Ru(NH_3)_6]^{3+/2+}$ redox mediator used as an ET probe. Importantly, we have observed consistent shifts between the anodic photocurrent onset potentials of thick and thin MoS_2 layers, which are explained by a difference in the work functions of bulk and monolayer MoS_2. The excellent photocorrosion stability and sensitivity of mono- and few-layer basal plane MoS_2 to extrinsic impurities, substrate identity, and illumination can be exploited in sensing and as a control of industrially important reactions, such as water oxidation, halide oxidation, and hydrogen evolution.

Methods. *Materials and Chemicals.* Hexaammineruthenium(III) chloride (98%), lithium chloride (99%), and potassium chloride (99%) were purchased from Sigma-Aldrich, U.K. and used as received. Aqueous solutions were prepared using deionized water (18.2 MΩ cm, Milli-Q Direct 8, Merck Millipore, U.S.A.). Cu, Ag, and Pt wires (>99.9%) were purchased from Advent Research Materials, U.K., and silver conductive paint was obtained from RS Components Ltd., U.K. The Ag/AgCl reference electrode was prepared by oxidation of a Ag wire in 0.1 M KCl. MoS_2 flakes were prepared by mechanical exfoliation of natural molybdenite crystals (Manchester Nanomaterials Ltd., U.K.) onto Si wafers (IBD Technologies, U.K.) spin-coated with ~100 nm layer of PMMA (MicroChem Corp, MA, U.S.A.).

MoS_2 Characterization. A Nikon Eclipse LV100ND optical microscope and a DS-Fi2 U3 CCD camera (Nikon Metrology, U.K. Ltd.) were used to visualize MoS_2 flakes and liquid droplets using bright-field and dark-field illumination modes. The microscope illumination power density (irradiance) was calibrated using the 843-R power meter with a NIST-calibrated 818-Sl Si photodiode (Newport Spectra-Physics Ltd., U.K.). Complementary Raman spectroscopy and PL measurement were used to assess the quality of the surface and obtained using an inVia spectrometer with unpolarized 532 nm laser excitation (<5 mW), 1800 grooves/mm grating and a 100× Leica objective (Renishaw plc, U.K.). AFM measurements were performed with a Bruker Dimension 3100 V instrument in tapping mode with the tip resonance frequency of ~350 kHz (see Supporting Figure S1 for example analysis). XPS spectra

DOI: 10.1021/acs.nanolett.5b05317
Nano Lett. 2016, 16, 2023−2032

acquisition and imaging was performed on an AXIS Nova instrument (Kratos Analytical Ltd., U.K.) and analyzed using CasaXPS software v.2.3 (Casa Software Ltd.).

Experimental Setup. MoS_2 flakes were electrically connected to a copper wire using a silver conductive paint and employed as working electrodes (WE) as shown in Figure 1C. Aqueous droplets of either 6 M LiCl electrolyte or redox mediator solution (3 mM $Ru(NH_3)_6Cl_3$ in 6 M LiCl) were formed using a borosilicate micropipette (ca. 1 μm internal tip diameter) and a pneumatic microinjector (PV820 Pneumatic PicoPump, WPI, U.S.A.). The high concentration of aqueous electrolyte (6 M LiCl) was necessary to prevent unwanted microdroplet evaporation and was validated in our previous work.[19,24,25,27,54] Vertical and horizontal motion of the micropipette with embedded Ag/AgCl reference electrode (RE) and Pt counter electrode (CE) was controlled using a MX7630 micromanipulator and a MC 1000e motion controller (Siskiyou, Oregon, U.S.A.). In this three-electrode configuration, the electron transfer and capacitance at the MoS_2/droplet interface were measured using potentiostats PGSTAT302N (Metrohm Autolab B.V., The Netherlands) and CompactStat.e (Ivium Technologies, The Netherlands), respectively, with the potential measured against an Ag/AgCl reference electrode in 6 M LiCl, which is ca. +0.19 V on the SHE scale. All measurements were performed at ambient temperature (21−25 °C).

■ ASSOCIATED CONTENT

Supporting Information

The Supporting Information is available free of charge on the ACS Publications website at DOI: 10.1021/acs.nanolett.5b05317.

Further MoS_2 characterization, illumination power density calibration, Raman and Pl spectra versus MoS_2 thickness calibration, high-resolution XPS spectra and XPS imaging of MoS_2, heterogeneity of Raman and PL spectra in monolayer MoS_2, dependence of electron transfer/capacitance on electrode area, intralayer resistance effects on ET kinetics, ET kinetics of individual MoS_2 samples, and dependence of capacitance on scan rate and illumination. (PDF)

■ AUTHOR INFORMATION

Corresponding Authors

*E-mail: matej.velicky@manchester.ac.uk. Tel: +44 (0)161-306-4522. Fax: +44 (0)161-275-4598.

*E-mail: robert.dryfe@manchester.ac.uk. Tel: +44 (0)161-306-4522. Fax: +44 (0)161-275-4598.

Notes

The authors declare no competing financial interest.

■ ACKNOWLEDGMENTS

The authors thank EPSRC (Grants EP/I005145/1 and EP/K016954/1) and BGT Materials Ltd. for funding, Dr. Jose Portoles at nanoLAB (Newcastle University) for XPS spectra and imaging measurements, Dr. Freddie Withers (Manchester University) for advice with sample preparation, and Dr. Andrew Rodgers and Dr. Hollie Patten (both Manchester University) for useful discussions.

■ REFERENCES

(1) Chhowalla, M.; Shin, H. S.; Eda, G.; Li, L. J.; Loh, K. P.; Zhang, H. *Nat. Chem.* **2013**, *5* (4), 263−275.

(2) Salomon, G.; De Gee, A. W. J.; Zaat, J. H. *Wear* **1964**, *7* (1), 87−101.

(3) Wang, Q. H.; Kalantar-Zadeh, K.; Kis, A.; Coleman, J. N.; Strano, M. S. *Nat. Nanotechnol.* **2012**, *7* (11), 699−712.

(4) Cui, X.; Lee, G.-H.; Kim, Y. D.; Arefe, G.; Huang, P. Y.; Lee, C.-H.; Chenet, D. A.; Zhang, X.; Wang, L.; Ye, F.; Pizzocchero, F.; Jessen, B. S.; Watanabe, K.; Taniguchi, T.; Muller, D. A.; Low, T.; Kim, P.; Hone, J. *Nat. Nanotechnol.* **2015**, *10* (6), 534−540.

(5) Ye, J. T.; Zhang, Y. J.; Akashi, R.; Bahramy, M. S.; Arita, R.; Iwasa, Y. *Science* **2012**, *338* (6111), 1193−1196.

(6) Kasowski, R. V. *Phys. Rev. Lett.* **1973**, *30* (23), 1175−1178.

(7) Splendiani, A.; Sun, L.; Zhang, Y.; Li, T.; Kim, J.; Chim, C.-Y.; Galli, G.; Wang, F. *Nano Lett.* **2010**, *10* (4), 1271−1275.

(8) Novoselov, K. S.; Jiang, D.; Schedin, F.; Booth, T. J.; Khotkevich, V. V.; Morozov, S. V.; Geim, A. K. *Proc. Natl. Acad. Sci. U. S. A.* **2005**, *102* (30), 10451−10453.

(9) Coleman, J. N.; Lotya, M.; O'Neill, A.; Bergin, S. D.; King, P. J.; Khan, U.; Young, K.; Gaucher, A.; De, S.; Smith, R. J.; Shvets, I. V.; Arora, S. K.; Stanton, G.; Kim, H. Y.; Lee, K.; Kim, G. T.; Duesberg, G. S.; Hallam, T.; Boland, J. J.; Wang, J. J.; Donegan, J. F.; Grunlan, J. C.; Moriarty, G.; Shmeliov, A.; Nicholls, R. J.; Perkins, J. M.; Grieveson, E. M.; Theuwissen, K.; McComb, D. W.; Nellist, P. D.; Nicolosi, V. *Science* **2011**, *331* (6017), 568−571.

(10) Jeon, J.; Jang, S. K.; Jeon, S. M.; Yoo, G.; Jang, Y. H.; Park, J.-H.; Lee, S. *Nanoscale* **2015**, *7* (5), 1688−1695.

(11) Al-Mamun, M.; Zhang, H.; Liu, P.; Wang, Y.; Cao, J.; Zhao, H. *RSC Adv.* **2014**, *4* (41), 21277−21283.

(12) Chang, K.; Chen, W. *ACS Nano* **2011**, *5* (6), 4720−4728.

(13) Lei, B.; Li, G. R.; Gao, X. P. *J. Mater. Chem. A* **2014**, *2* (11), 3919−3925.

(14) Bissett, M. A.; Kinloch, I. A.; Dryfe, R. A. W. *ACS Appl. Mater. Interfaces* **2015**, *7* (31), 17388−17398.

(15) Voiry, D.; Salehi, M.; Silva, R.; Fujita, T.; Chen, M.; Asefa, T.; Shenoy, V. B.; Eda, G.; Chhowalla, M. *Nano Lett.* **2013**, *13* (12), 6222−6227.

(16) Tributsch, H.; Bennett, J. C. *J. Electroanal. Chem. Interfacial Electrochem.* **1977**, *81* (1), 97−111.

(17) Ahmed, S. M. *Electrochim. Acta* **1982**, *27* (6), 707−712.

(18) Tan, S. M.; Ambrosi, A.; Sofer, Z.; Huber, Š.; Sedmidubský, D.; Pumera, M. *Chem. - Eur. J.* **2015**, *21* (19), 7170−7178.

(19) Velický, M.; Bissett, M. A.; Toth, P. S.; Patten, H. V.; Worrall, S. D.; Rodgers, A. N. J.; Hill, E. W.; Kinloch, I. A.; Novoselov, K. S.; Georgiou, T.; Britnell, L.; Dryfe, R. A. W. *Phys. Chem. Chem. Phys.* **2015**, *17* (27), 17844−17853.

(20) Wang, Y.; Ou, J. Z.; Balendhran, S.; Chrimes, A. F.; Mortazavi, M.; Yao, D. D.; Field, M. R.; Latham, K.; Bansal, V.; Friend, J. R.; Zhuiykov, S.; Medhekar, N. V.; Strano, M. S.; Kalantar-Zadeh, K. *ACS Nano* **2013**, *7* (11), 10083−10093.

(21) Chia, X.; Ambrosi, A.; Sedmidubský, D.; Sofer, Z.; Pumera, M. *Chem. - Eur. J.* **2014**, *20* (52), 17426−17432.

(22) Yu, Y.; Huang, S.-Y.; Li, Y.; Steinmann, S. N.; Yang, W.; Cao, L. *Nano Lett.* **2014**, *14* (2), 553−558.

(23) Li, W.; Tan, C.; Lowe, M. A.; Abruña, H. D.; Ralph, D. C. *ACS Nano* **2011**, *5* (3), 2264−2270.

(24) Velický, M.; Bradley, D. F.; Cooper, A. J.; Hill, E. W.; Kinloch, I. A.; Mishchenko, A.; Novoselov, K. S.; Patten, H. V.; Toth, P. S.; Valota, A. T.; Worrall, S. D.; Dryfe, R. A. W. *ACS Nano* **2014**, *8* (10), 10089−10100.

(25) Velický, M.; Cooper, A. J.; Toth, P. S.; Patten, H. V.; Woods, C. R.; Novoselov, K. S.; Dryfe, R. A. W. *2D Mater.* **2015**, *2* (2), 024011.

(26) Güell, A. G.; Cuharuc, A. S.; Kim, Y.-R.; Zhang, G.; Tan, S.-y.; Ebejer, N.; Unwin, P. R. *ACS Nano* **2015**, *9* (4), 3558−3571.

(27) Toth, P. S.; Valota, A.; Velický, M.; Kinloch, I.; Novoselov, K.; Hill, E. W.; Dryfe, R. A. W. *Chem. Sci.* **2014**, *5* (2), 582−589.

DOI: 10.1021/acs.nanolett.5b05317
Nano Lett. 2016, 16, 2023−2032

(28) Bard, A. J.; Faulkner, L. R. *Electrochemical Methods. Fundamentals and Applications*, 2nd ed.; John Wiley & Sons, Inc.: New York, 2001.
(29) Dolui, K.; Rungger, I.; Sanvito, S. *Phys. Rev. B: Condens. Matter Mater. Phys.* **2013**, *87* (16), 165402.
(30) Li, H.; Zhang, Q.; Yap, C. C. R.; Tay, B. K.; Edwin, T. H. T.; Olivier, A.; Baillargeat, D. *Adv. Funct. Mater.* **2012**, *22* (7), 1385−1390.
(31) Frindt, R. F. *J. Appl. Phys.* **1966**, *37* (4), 1928−1929.
(32) Lee, C.; Yan, H.; Brus, L. E.; Heinz, T. F.; Hone, J.; Ryu, S. *ACS Nano* **2010**, *4* (5), 2695−2700.
(33) Klingler, R. J.; Kochi, J. K. *J. Phys. Chem.* **1981**, *85* (12), 1731−1741.
(34) Nicholson, R. S. *Anal. Chem.* **1965**, *37* (11), 1351−1355.
(35) Lavagnini, I.; Antiochia, R.; Magno, F. *Electroanalysis* **2004**, *16* (6), 505−506.
(36) Dolui, K.; Rungger, I.; Das Pemmaraju, C.; Sanvito, S. *Phys. Rev. B: Condens. Matter Mater. Phys.* **2013**, *88* (7), 075420.
(37) Zhou, W.; Zou, X.; Najmaei, S.; Liu, Z.; Shi, Y.; Kong, J.; Lou, J.; Ajayan, P. M.; Yakobson, B. I.; Idrobo, J.-C. *Nano Lett.* **2013**, *13* (6), 2615−2622.
(38) Baugher, B. W. H.; Churchill, H. O. H.; Yang, Y.; Jarillo-Herrero, P. *Nano Lett.* **2013**, *13* (9), 4212−4216.
(39) Late, D. J.; Liu, B.; Matte, H. S. S. R.; Dravid, V. P.; Rao, C. N. R. *ACS Nano* **2012**, *6* (6), 5635−5641.
(40) McDonnell, S.; Addou, R.; Buie, C.; Wallace, R. M.; Hinkle, C. L. *ACS Nano* **2014**, *8* (3), 2880−2888.
(41) Bao, W.; Cai, X.; Kim, D.; Sridhara, K.; Fuhrer, M. S. *Appl. Phys. Lett.* **2013**, *102* (4), 042104.
(42) Tonndorf, P.; Schmidt, R.; Böttger, P.; Zhang, X.; Börner, J.; Liebig, A.; Albrecht, M.; Kloc, C.; Gordan, O.; Zahn, D. R. T.; De Vasconcellos, S. M.; Bratschitsch, R. *Opt. Express* **2013**, *21* (4), 4908−4916.
(43) Bernardi, M.; Palummo, M.; Grossman, J. C. *Nano Lett.* **2013**, *13* (8), 3664−3670.
(44) Liu, J.-T.; Wang, T.-B.; Li, X.-J.; Liu, N.-H. *J. Appl. Phys.* **2014**, *115* (19), 193511.
(45) Son, Y.; Wang, Q. H.; Paulson, J. A.; Shih, C.-J.; Rajan, A. G.; Tvrdy, K.; Kim, S.; Alfeeli, B.; Braatz, R. D.; Strano, M. S. *ACS Nano* **2015**, *9* (3), 2843−2855.
(46) Xiong, G.; Meng, C.; Reifenberger, R. G.; Irazoqui, P. P.; Fisher, T. S. *Electroanalysis* **2014**, *26* (1), 30−51.
(47) Rice, R. J.; Pontikos, N. M.; McCreery, R. I. *J. Am. Chem. Soc.* **1990**, *112* (12), 4617−4622.
(48) Rice, R. J.; McCreery, R. L. *Anal. Chem.* **1989**, *61* (15), 1637−1641.
(49) Liu, Y.; Chen, S. *J. Electroanal. Chem.* **2015**, *753*, 3−8.
(50) Tributsch, H. *Faraday Discuss. Chem. Soc.* **1980**, *70*, 189−205.
(51) Kubiak, C. P.; Schneemeyer, L. F.; Wrighton, M. S. *J. Am. Chem. Soc.* **1980**, *102* (22), 6898−6900.
(52) Britnell, L.; Ribeiro, R. M.; Eckmann, A.; Jalil, R.; Belle, B. D.; Mishchenko, A.; Kim, Y.-J.; Gorbachev, R. V.; Georgiou, T.; Morozov, S. V.; Grigorenko, A. N.; Geim, A. K.; Casiraghi, C.; Neto, A. H. C.; Novoselov, K. S. *Science* **2013**, *340* (6138), 1311−1314.
(53) Kline, G.; Kam, K. K.; Ziegler, R.; Parkinson, B. A. *Sol. Energy Mater.* **1982**, *6* (3), 337−350.
(54) Valota, A. T.; Toth, P. S.; Kim, Y. J.; Hong, B. H.; Kinloch, I. A.; Novoselov, K. S.; Hill, E. W.; Dryfe, R. A. W. *Electrochim. Acta* **2013**, *110*, 9−15.

DOI: 10.1021/acs.nanolett.5b05317
Nano Lett. 2016, 16, 2023−2032